ELSEVIER

Chemical Engineering Journal 132 (2007) 47–59

Chemical Engineering Journal

www.elsevier.com/locate/cej

Trickle flow distribution and stability by X-ray radiography

Werner van der Merwe [a], Willie Nicol [a,*], Frikkie de Beer [b]

[a] *Department of Chemical Engineering, University of Pretoria, Pretoria 0002, South Africa*
[b] *SANRAD, South African Nuclear Energy Corporation, Pelindaba, South Africa*

Received 27 September 2006; received in revised form 11 January 2007; accepted 13 January 2007

Abstract

The distribution of the fluid phases in trickle beds is usually investigated using visualization techniques like computed tomography or colorimetrics or with annular collecting devices. These experimental techniques suffer from an inability to provide data at a spatial and temporal resolution suitable for investigating the stability of the liquid flow pattern at the particle scale. Presently, rapidly acquired X-ray radiographs are used to shed new light on various aspects of trickle flow. Radiography derived liquid saturation values of a section of the bed correspond closely to gravimetrically determined saturations. It is demonstrated that the flow patterns encountered in multiple hydrodynamic states can be successfully visualized using X-ray radiography. Trickle flow is stable in all but one of the pre-wetting modes investigated. In the Levec mode, low frequency particle scale instability exists at sparsely dispersed locations in the bed. Although both the type of flow pattern and the liquid saturation are reproducible, the actual flow patterns themselves are shown not to be. In general, the stability of the flow pattern validates the use of tomographic and colorimetric methods for investigating trickle flow hydrodynamics.

Keywords: Trickle flow stability; Multiple hydrodynamic states

1. Introduction

Trickle bed reactors are catalytic gas–liquid–solid reactors in which the fluids are fed co-currently downward over a packed bed of stationary particles. The hydrodynamics of trickle beds has come under intensive investigation over the last five decades. In the trickle flow regime (which is encountered at relatively low fluid velocities), bed-averaged hydrodynamic parameters like liquid saturation (or liquid holdup) and pressure drop have been used extensively to characterize the hydrodynamic condition of the reactor [1]. More recently, visualization techniques like colorimetry [2–5] and computed tomography [6–18] have provided insights into localized trickle flow phenomena. In particular, the structure of packed beds and the distribution of the fluid phases in these beds on various scales and under differing circumstances have been given considerable attention. Unfortunately, these techniques suffer from experimental constraints that make them unsuitable for the investigation of certain aspects of trickle flow hydrodynamics. In this study, the ability of X-ray radiography to address some of the unresolved issues is demonstrated. To qualify these issues, brief overviews of existing visualization techniques follow.

The colorimetric technique involves colouring the catalyst particles at the locations where the liquid is in contact with the particle surface. The trickle flow is brought to steady state before the feed is switched to a dye solution for either 5 or 20 min [2–5]. The wetting efficiency is calculated directly from the (partially) coloured particles, while the liquid distribution can be inferred from such data [5]. The validity of the technique is dependent upon the assumption that the liquid distribution remains stable throughout the period of dye irrigation. Any flow path deviations during this time will result in non-uniformly coloured particles and probably an over-estimation of the wetting efficiency and the flow uniformity. A further drawback of this method is its intrusive nature. The feed properties are changed by the dye and there are flow rate disturbances that influence the flow stability [13] and potentially the liquid distribution.

In computed tomography (CT), the bed is subjected to some form of radiation (γ-, X- or neutron) or a magnetic field (MRI) at several angles of rotation. Other tomographic techniques exist, but they have not been used specifically to investigate trickle flow hydrodynamics. CT yields a three-dimensional reconstruction of the entire volume under consideration. In terms of trickle

* Corresponding author. Tel.: +27 12 420 3796; fax: +27 12 362 5173.
E-mail address: willie.nicol@up.ac.za (W. Nicol).

1385-8947/$ – see front matter © 2007 Elsevier B.V. All rights reserved.
doi:10.1016/j.cej.2007.01.015

Nomenclature

D	column diameter (cm)
E	liquid attenuation (m^{-1})
G	superficial gas flux (kg/m^2 s)
H	packing height (cm)
i	pixel number
I	image intensity (arbitrary)
I_0	free field image intensity (arbitrary)
L	superficial liquid flux (kg/m^2 s)
Δs	spatial resolution (m)
$V_{section}$	volume of the bed section under investigation (m^3)
x	liquid thickness transverse to the viewing plane (m)

Greek letter

ε	external porosity

flow CT, the liquid distribution has been successfully investigated (for selected conditions) by several authors [6,7,9,13–18]. However, CT investigations also assume that the flow remains stable during the acquisition of the images required for the volume reconstruction. These acquisition times can be very short (ms) if one is prepared to accept either relatively poor spatial resolution (mm, MRI) or reconstruction artefacts in the final volume image (for example "streak lines" in X-ray tomography). For a greater resolution MRI image of a dry bed (μm), Anadon et al. [12] used an acquisition time of 11.5 h, but they do not report such high resolution images for trickle flow conditions. Gladden et al. [13] conducted a stability analysis of trickle flow using 2D images with acquisition times of 30 s per image and an in-plane resolution of 352 μm per pixel. For radiation-based CT, longer acquisition times will be required for larger diameter beds. A summary of CT and radiography investigations (with pertinent experimental conditions) into the trickle flow regime is given in Table 1. The trade-off between spatial resolution and acquisition time means that sufficiently high frequency flow path deviations can either not be detected (for the radiation-based CT, i.e. long acquisition times) or cannot be detected with a resolution smaller than a few millimetres per voxel (e.g. MRI). Note that there are three beam geometries for X- or γ-ray tomography. If fan beam geometry is used, it is possible to acquire rapid 2D cross-sectional images, but the question remains whether these are representative of the entire bed. Parallel beam geometry allows relatively rapid acquisition of radiographs, but no geometric enlargement of the sample. Cone beam geometry allows rapid radiograph acquisition as well as geometric enlargement of the sample, but introduces an element of inaccuracy called unsharpness.

An additional technique employed in determination of liquid distribution is that of the annular collector installed at the bottom of the bed [4,21]. The liquid flux through each annular region is measured. The size and geometry of the annular regions are chosen rather arbitrarily and the minimum size of each region is limited by practical constraints. In this technique, the data represent the time-averaged bottom-of-bed liquid flux distribution.

It is evident from the preceding discussion that there is a need for determining the stability of trickle flow with high spatial and temporal resolutions. A proper interpretation of computed tomographical reconstructions and colorimetric data is depen-

Table 1
Trickle flow CT and radiation studies in literature

Reference	Type	Bed size ($D \times H$) (cm)	Packing	Pre-wetting methods	Spatial resolution (μm)	TSS (min)	Acquisition time (s)
[6]	X-ray	6.03 × 19.05	Glass spheres	NPW and Kan-Liq	500	n.r.	26 (2D)
[15]	Capacitance	12 × 200	Celcore spheres	NA	6000–12,000	n.r.	0.01 (2D)
[14]	X-ray	4.5 × 45	Glass spheres	NPW	400 × 400 × 3000	n.r.	450 (3D[a])
[7][b]	X-ray	80 × 200	Polypropylene wheels	n.r.	880	n.r.	150 (3D[a])
[16]	X-ray	20 × 25	Ceramic spheres	NPW and pre-wetted	400	n.r.	900 (3D[a])
[8]	MRI	4 × 55	Extrudate and spheres	NPW	313	160	n.r.
[9]	MRI	4 × 50	Glass ballotini	NPW and Levec	328	n.r.	21,600 (3D[a]), 180 (2D)
[17]	γ-ray	60 × 60	Pall rings	n.r.	n.r.	n.r.	n.r.
[18]	MRI	4 × 50	Alumina extrudate	Wetted	156	n.r.	1500 (2D)
[10]	γ-ray	60 × n.r.	Alumina extrudate	n.r.	n.r.	n.r.	2700 (2D)
[11][b]	X-ray	60 × 200	Polypropylene packing	n.r.	1000	n.r.	160 (2D)
[13]	MRI	70 × 4.5	Porous cylinders	n.r.	352	n.r.	30 (2D)
[19,20]	X-ray	17 × 6 (rectangular), 75 (height)	Polystyrene spheres	NPW	757 × 757 × 60,000	15	900 (2D)
[12]	MRI	4.3 × 70	Porous extrudate	Levec	3750 × 3750 × 1870 or 175 × 175 × 175	n.r.	0.28 (3D[a]) or 41,400 (3D[a])

n.r.: not reported, TSS: time to reach steady state.
[a] 3D images are obtained by stacking 2D images (obtained at several axial locations) on top of one another.
[b] These authors investigated structured packings.

dent upon the knowledge of whether or not the volume images or coloured regions are time-averaged representations of liquid and gas distributions or in fact a stable phase distribution configuration. In this study, cone beam X-ray radiography is used to study the temporal stability of trickle flow. Radiography is better suited to the investigation of liquid saturation in porous media because it does not require exact phase-border distinction in order to attain phase saturations (X-ray CT for example requires the reconstructed image to be thresholded to distinguish between liquid, gas and solid—see Boyer and Fanget [10] for the various errors that can be introduced in tomographical acquisition and reconstruction). Liquid saturation is usually defined as the volumetric fraction of the void space that is occupied by liquid. X-ray radiography has been used successfully to study both liquid saturation and distribution in trickle flow packed beds [19,20].

The present investigation is concerned specifically with the existence of multiple hydrodynamic states in the trickle flow regime. For given operating conditions it has been shown that macroscopic hydrodynamic parameters can adopt many different values at steady state [20–27]. The exact values are functions of the phase distributions, which in themselves are functions of the gas and liquid flow histories [9,26]. Adopting the approach of Wang et al. [26] (most recently extended by Loudon et al. [27] to include all flow rate variations), it is assumed that all hydrodynamic states fall within the bounds of specifically defined pre-wetting procedures, these being:

(1) non-pre-wetted (NPW);
(2) Levec pre-wetted (flooded and drained, followed by liquid introduction);
(3) Kan pre-wetted with liquid (Kan-Liq: pre-wetted, operated in the pulsing flow regime by increasing L at constant G, followed by decreasing L to its operating value);
(4) Kan pre-wetted with gas (Kan-Gas: pre-wetted, operated in the pulsing flow regime by increasing G at constant L, followed by decreasing G to its operating value);
(5) Super pre-wetted (flooding, introducing liquid as draining commences);
(6) an experimental investigation into the behaviour of macroscopic hydrodynamic parameters in each of these operational modes can be found in Loudon et al. [27]. Existing literature on trickle flow stability apparently considered only one of these operating modes [13,8]. Although potentially substantial, the impact of operating reactive applications in these various modes has not been established.

In simple terms the focus here is to:

- Compare radiography and gravimetry as tools for a hydrodynamic investigation of trickle flow.
- Visualize the flow patterns encountered in different hydrodynamic states.
- Determine whether trickle flow is stable locally in the bed. In particular, to illustrate the usefulness of rapidly acquired radiographs to analyse the liquid distribution and its dynamic behaviour. There is some discrepancy as to the time it takes (from start-up) to reach steady state. This start-up time appears to vary considerably depending on the pre-wetting procedure [4]. The start-up dynamics are therefore also investigated.
- Establish whether the flow distributions and liquid saturations are reproducible provided that the same pre-wetting procedure was followed.

A number of studies have been concerned with the distribution of liquid and the degree of non-uniformity of this distribution [9,19–21,26,28,29]. The radiographic technique employed here provides visualizations of the overall liquid distribution in the bed for different fluid velocities and pre-wetting histories. It is the purpose of this study to illustrate how a relatively simple technique can provide new insights into trickle flow phenomena. X-ray radiography has the potential to be scaled up to larger applications with relative ease [11] (although the presence of steel reactor walls in industry diminishes this scaling ability). It is therefore imperative to investigate its capabilities with regards to the issues of flow stability and the effects of pre-wetting.

2. Experimental

A comprehensive description of the experimental facility as pertains to the acquisition of radiographs is given elsewhere [30]. Fig. 1 is a schematic of the set-up. The 40 mm (inner diameter) polypropylene column is mounted on a stand. The column is packed with spherical porous γ-alumina catalyst particles of diameter 2.5 mm. Air and water (atmospheric conditions) at controlled flow rates are fed co-currently downward into the bed. These fluids are used for ease of implementation and

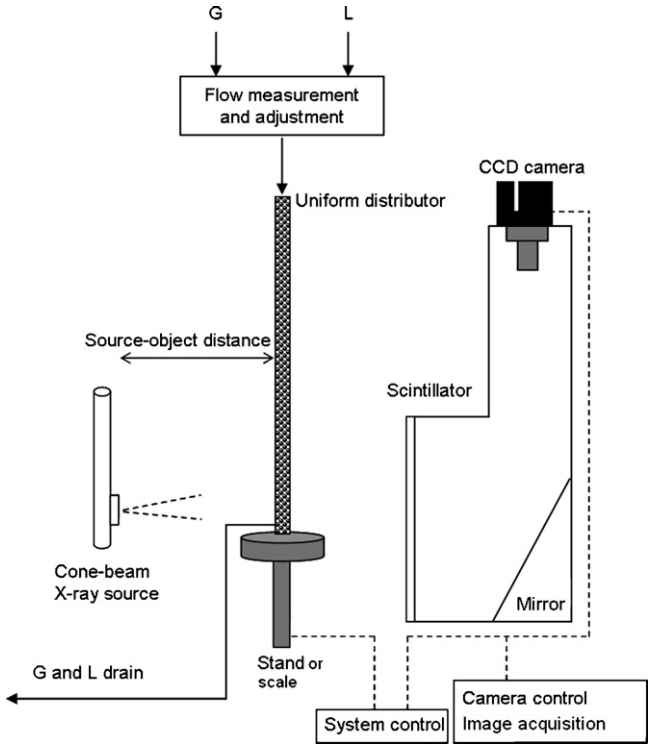

Fig. 1. Experimental set-up.

Table 2
Experimental parameters

X-ray source	Tungsten filament
X-ray voltage	100 keV (at 6 mA)
Packing	2.5 mm γ-alumina spheres (porous)
Packing height	900 mm
Exposure time	1.5 s per radiograph
Delay time (between successive acquisitions)	Approximately 0.5 s
Image size (binning)	512 × 512 pixels (2)
Spatial resolution	120 μm/pixel (approximately)
Focal point opening	1 mm
Source object distance (SOD)	610 mm

are the most common fluids found in the trickle bed literature. Experimental gas and liquid fluxes were chosen to represent a wide range of conditions within the trickle flow regime. Liquid fluxes varied from 1.3 to 8.0 kg/m^2 s and gas fluxes from 0 to 0.16 kg/m^2 s. The liquid is distributed uniformly at the top of the bed through 16 equally sized and equally spaced holes; resulting in a drip point density in excess of 10 000 points/m^2. This ensures that the liquid distribution in the bed is independent of the distributor [31]. A uniform initial distribution has been shown to be crucial to achieving proper liquid distribution inside the bed [4]. The gas enters the bed through a separate 1/4 in. tube located in the centre of the distributor head. For the pre-wetted modes, the bed was flooded for 5 h prior to experimentation to ensure complete internal saturation of the catalyst spheres [32].

Experimental considerations with regards to the acquisition of X-ray radiographs are the amplitude of the X-ray source, the focal point size, the source–detector distance and the presence of inorganic species in the liquid phase [7,20,29]. Extensive testing during the course of this investigation revealed that the experimental conditions listed in Table 2 yield satisfactory results. Note that adequate phase distinction was achieved without the need to add $BaCl_2$. This ensures that the liquid properties were not changed from that of water, reduces beam hardening and reduces deviations from the Beer–Lambert law (as discussed later).

Using these settings, a radiograph of 61 mm of the bed was obtained. The top of the radiographed section was located 539 mm below the top of the bed. This was done specifically to avoid the calming zone at the top of the bed where the liquid distribution is not representative of the entire bed [33].

As in Basavaraj et al. [19], the beam hardening effect is minimized by two measures:

- A low inorganic concentration (in the present study no salt was added to the liquid).
- A hardware filter (in the present study the 5 mm polyethylene column walls acted as a filter for the incoming X-rays).

Representative radiographs are shown in Fig. 2. These images were filtered using a 3 × 3 low pass filter in order to remove experimental noise (white spots). In Fig. 2(a), the column had not been placed in the X-ray beam. The cone beam geometry is evident from the fact that the image intensity is higher in the centre of the image and decreases towards the sides. Fig. 2(b) is the radiograph of the column packed with dry particles. Note that the X-rays traverse the entire diameter (50 mm) of the column only in the centre of the image. As one moves away from the central vertical axis, the intensity increases because the X-rays pass through less material (because of the cylindrical shape of the column) and are therefore not as severely attenuated. The reduction in intensity in the image is related to the thickness of material transverse to the viewing plane. Fig. 2(c) is the same column after the introduction of liquid (non-pre-wetted mode). The darkening of the image is indicative of the beam being attenuated by the water in the bed. Similarly, radiographs of a pre-wetted and drained bed (no flow) and a bed in the different pre-wetting modes can be obtained once the flow had stabilized.

There is a geometrical error in these radiographs that stem from the cone geometry of the X-ray beam. X-rays travelling to the top (and bottom) of the image section has a slightly longer path length (and therefore diverges more than those travelling in the plane of the focal point). This results in the top (and bottom) of the image appearing slightly larger than the middle. In the present investigation, this error is negligible because the source–object distance greatly exceeds the size of the sample. The apparent size of the top (and bottom) of the column is approximately 0.5% larger than the apparent size of the middle.

The intensity of the attenuated image (I) relates to the intensity of a free field image (I_0) according to the Beer–Lambert law [7,19,20]:

$$I = I_0 \, \mathrm{e}^{-Ex} \tag{1}$$

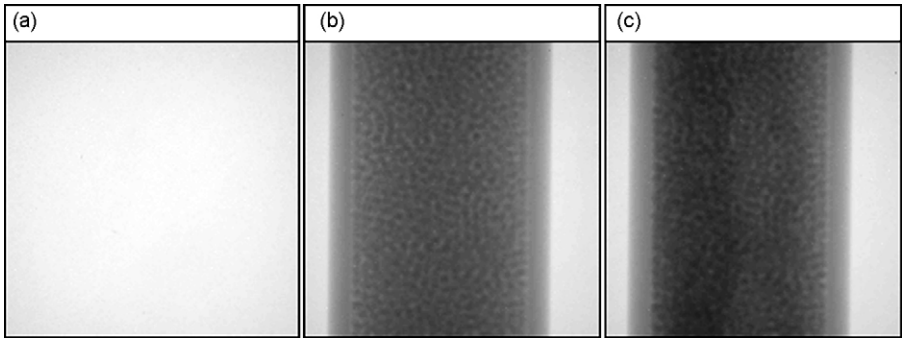

Fig. 2. A selection of radiographs: (a) free field; (b) dry bed; (c) non-pre-wetted bed.

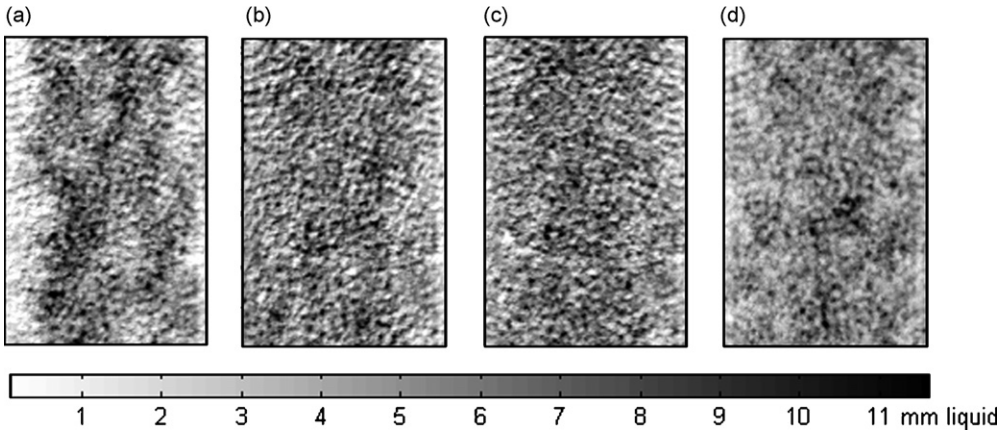

Fig. 3. Liquid distribution in the various pre-wetting modes ($L = 8.0\,kg/m^2\,s$ and $G = 0.016\,kg/m^2\,s$): (a) Levec; (b) Kan-Liq; (c) Kan-Gas; (d) Super.

Here x is the thickness of the attenuating material and E is the attenuation coefficient (assumed to be independent of x). For a given fluid, E is a function of the voltage of the X-ray source. At 100 keV its value is 17.07 m^{-1} for water [34]. Several processing combinations are possible. Using Fig. 2(a) as the free field image (I_0) and (b) as the intensity image (I), the solids content in the bed is isolated. Alternatively, setting Fig. 2(b) as I_0 and (c) as I, the water content in the bed at the time of acquisition is obtained. This however, includes the internal holdup. For pre-wetted beds, the pre-wetted and drained bed is set as I_0 and the irrigated bed as I, yielding the dynamic (more accurately the free-draining) holdup in the bed during operation at the time of acquisition. An example of a Levec mode of operation is shown in Fig. 3(a). Here, the (dark) intensity of the image is proportional to the thickness of water transverse to the viewing plane. Since the exposure time for such an image is equal to 1.5 s, the image actually shows the average water thicknesses in the preceding 1.5 s. However, for practical purposes it can be thought of as a snapshot of the liquid in the bed at the time of acquisition. Images similar to that shown in Fig. 3(a) were generated for all times (at intervals of 2 s), fluid velocities and operating modes (e.g. Fig. 3(b)–(d)). They are used to characterize the stability and uniformity of the flow. Note that any changes in the total amount of liquid in the column or in the distribution of the liquid in the column will register on these images. To re-iterate, the dark intensity in Fig. 3 is the thickness of liquid transverse to the viewing plane. It represents the entire bed and not just the wall flow or a vertical slice of the bed as one would get from a tomographical reconstruction (as originally reported in Lutran et al. [6]).

3. Comparison between radiographic and gravimetric saturation values

3.1. Liquid saturation from radiographs

The liquid saturation (holdup divided by the external porosity) in the field of view of the radiograph is determined from images analogous to those in Fig. 3 by summation of the water thickness at each location, i.e.:

$$\text{dynamic saturation} = \frac{\sum_{\text{all pixels}} x_i \Delta s^2}{V_{\text{section}} \varepsilon} \quad (2)$$

The saturation obtained through this radiographic technique may be inaccurate because of:

- The presence of several processing steps (in arriving at Fig. 3) and in particular the assumption of a constant attenuation coefficient (E). Improved saturation values can be obtained through a calibration technique [19–29], but the subsequent qualitative investigations into flow stability are not expected to be affected by assuming E to be constant.
- The liquid saturation is only applicable to a section of 61 mm of a 900 mm bed.
- Any high frequency oscillations that occur within the 1.5 s of exposure time will register as averaged intensity values.

With regards to liquid distribution, the drawback of radiography (as opposed to tomography) is evident from Eq. (1). While the amount (thickness, x) of the liquid in the direction transverse to the image can be obtained (by solving for x in Eq. (1)), all the information on how the liquid is distributed in that direction is lost. Nevertheless, the different flow patterns can still be distinguished (compare Fig. 3(a)–(d)). Note also, that any flow fluctuation will be registered as an increase (darkening, increased saturation) or decrease (lighting, decreased saturation) in the intensity at a location.

3.2. Gravimetric saturation determination

It is imperative to compare the radiographic interpretation presented here to gravimetric saturation measurements. Since there is a considerable scatter in liquid saturation measurements in literature due to system and operating differences, liquid saturation was measured under conditions similar to those under which the radiographs were taken. Due to practical constraints, the liquid saturation measurement was not done during the actual radiography experiment. Instead, the set-up was moved

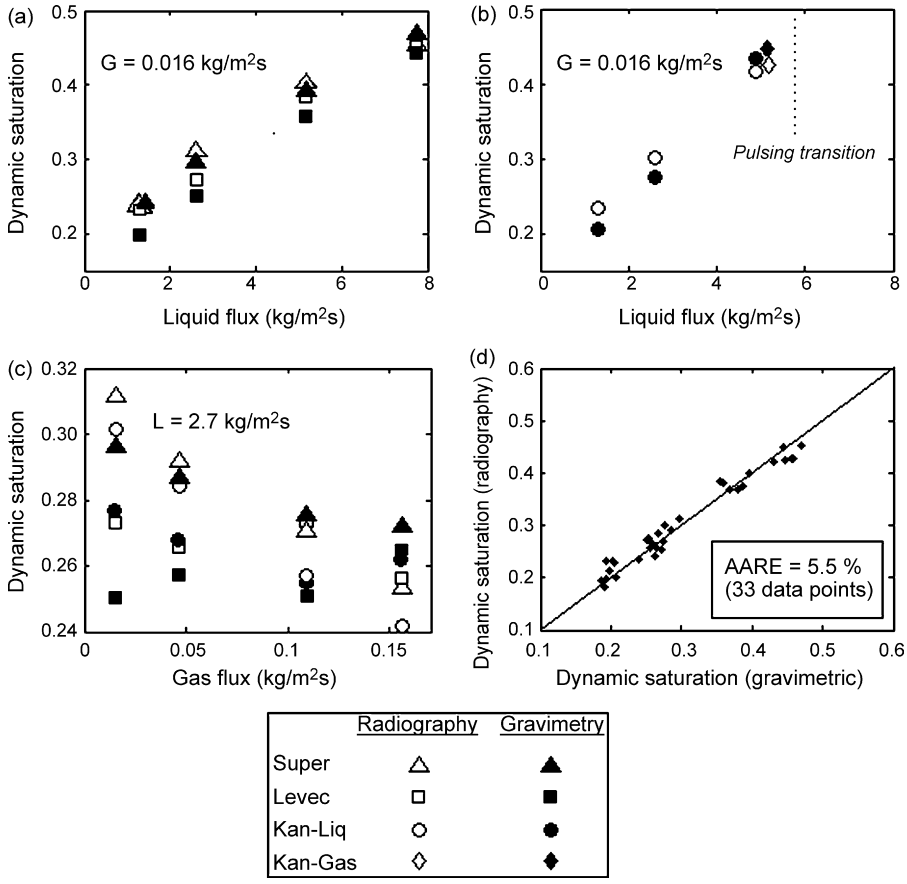

Fig. 4. Gravimetric and radiographic saturation comparisons: (a) Levec and Super; (b) Kan-Liq and Kan-Gas; (c) all modes vs. gas flow; (d) parity plot.

to another location where the column was mounted on an Ohaus Pro 22001 balance that is capable of registering intervals of 0.1 g in mass. Identical operating procedures were followed for the radiographic and gravimetric experiments. The procedure for determining liquid saturation by gravimetric means involves subtracting the weight of the drained bed from an irrigated bed and is discussed in detail elsewhere [35]. Gravimetric saturation measurements were found to be satisfactorily reproducible. Unfortunately, the bed had to be re-packed between the two sets of experiments. However, the bed porosity was found to be very reproducible with re-packing (a value of 0.41 is used throughout this study). Additionally, it was necessary to correct the measurements for significant hysteresis in the amount of water retained in the distributor. In order to properly evaluate the temporal evolution of the liquid saturation, the weight of liquid present in the bed was recorded every second from start-up to steady state (and beyond) for each mode of operation.

Possible inaccuracies in the gravimetric method of gravimetric determination described here are:

- End effects (including the liquid in the distributor and retained on top of the sieve at the bottom of the bed).
- The gravimetrically determined liquid saturation is a bed-averaged value and therefore includes the non-representative calming zone holdup that may well encompass the first 400 mm of the bed [33].

The gravimetric liquid saturation measurements serve as a check of the radiographic technique employed here. One would expect the two methods to give similar liquid saturation values at steady state. A selection of results is shown in Fig. 4(a)–(c). Note that both techniques indicate that liquid saturation increases with liquid flux (Fig. 4(a) and (b)) and decreases with gas flux (Fig. 4(c)). Fig. 4(d) is a parity plot of the liquid saturation at all fluid velocities and all pre-wetting modes as determined by the radiographic and gravimetric techniques. An average absolute relative error (AARE) of 5.5% indicates that there is excellent agreement between the two techniques, especially considering that a constant attenuation coefficient was used.

4. Results and discussion

4.1. Liquid configuration variation with fluid fluxes

The radiographic technique is suitable for a visualization of the liquid flow pattern. Fig. 5 shows processed radiographs of the bed at steady state for different liquid and gas fluxes. Note that the higher fluxes reported do not imply that the bed was operated at the low flux and that the flux was then increased. Instead, for the Levec mode, the bed was pre-wetted and drained and then the operating fluxes were introduced. If a higher operating value was required, the whole procedure was repeated. For the Kan-Liq mode the operating fluxes were

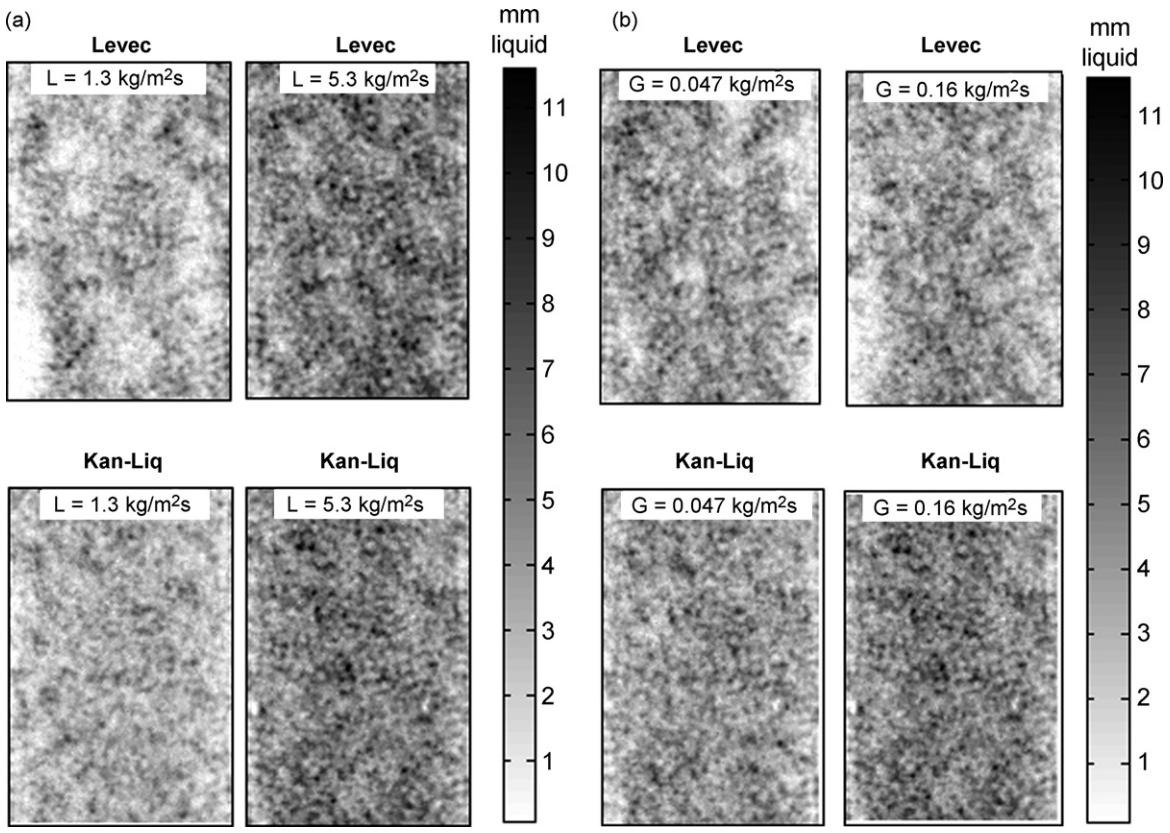

Fig. 5. Flow patterns with increased fluid fluxes: (a) $G = 0.047\,kg/m^2\,s$; (b) $L = 2.7\,kg/m^2\,s$.

set, the liquid flow was increased and then decreased to the operating value—again repeating the whole procedure if higher fluxes were required. Similarly, the Super bed was flooded between flow rate changes and the Kan-Gas bed was pulsed (with increased gas flow) between flow rate changes (their results were similar to the Kan-Liq mode and are not shown). Examination of Fig. 5(a) suggests that in the Levec mode the liquid is improperly distributed through the volume (areas of dark and light) while in the Kan-Liq mode the liquid is relatively uniformly distributed. Moreover, the improper distribution in the Levec mode persists at high liquid velocities. Finally, it appears as though the there are completely dry zones at the low L (see for example the lower left corner of the image). Although there is still improper distribution at high L, the completely dry zone is absent. This is in agreement with Sederman and Gladden [9] who reported that there is new rivulet creation as L is increased up to $2\,kg/m^2\,s$, as well as Van der Merwe and Nicol [36] and Van Houwelingen et al. [5] who report completely dry zones at low L. From Fig. 5(b) it is not clear what the effect of gas flow is on the liquid morphology. It is apparent however, that the improper liquid distribution in the Levec mode persists at high gas velocity and even appears to increase as a result of the higher gas flux. This is contrary to the expectation that high gas fluxes will serve to spread the liquid more evenly over the packing. Unexpectedly, there are several dark spots (local volumes of high liquid saturation) in the Kan-Liq mode at high G that are not as apparent at lower G. Here the gas may indeed have the expected effect of increasing the liquid spreading [37]. In accordance with this, a higher total liquid saturation is registered at this higher G (Fig. 4(c)). It is noted that an increased wetting efficiency as a result of increased gas flux was reported for this pre-wetting mode by Al-Dahhan and Dudukovic [37], which certainly indicates better liquid spreading (although their saturation decreased with gas velocity). However, present results pertain to low pressure conditions (although the gas density is $1.1\,kg/m^3$). It is advisable to investigate this issue under elevated pressures where such effects may be more pronounced.

A mathematical analysis based on the calculation of maldistribution factors for these radiographic images is inappropriate. This is because all the information regarding the liquid distribution transverse to the viewing plane is lost. The maldistribution factor would therefore be insensitive to changes in liquid morphology in that direction. In addition, due to the cylindrical column shape, a small change in the liquid morphology close to the wall (in the viewing plane) will drastically affect the factor, while even a substantial change to the flow morphology close to the centre of the column (in the viewing plane) will fail to affect it significantly. Maldistribution is therefore better investigated in quantitative terms by computed tomography.

4.2. Start-up dynamics

Little attention has been given to the time required (from start-up) for the liquid saturation to reach its steady state value (see Table 1). Ravindra et al. [4] reported that the time-to-steady-state (TSS) can vary from 10 to 360 min depending upon

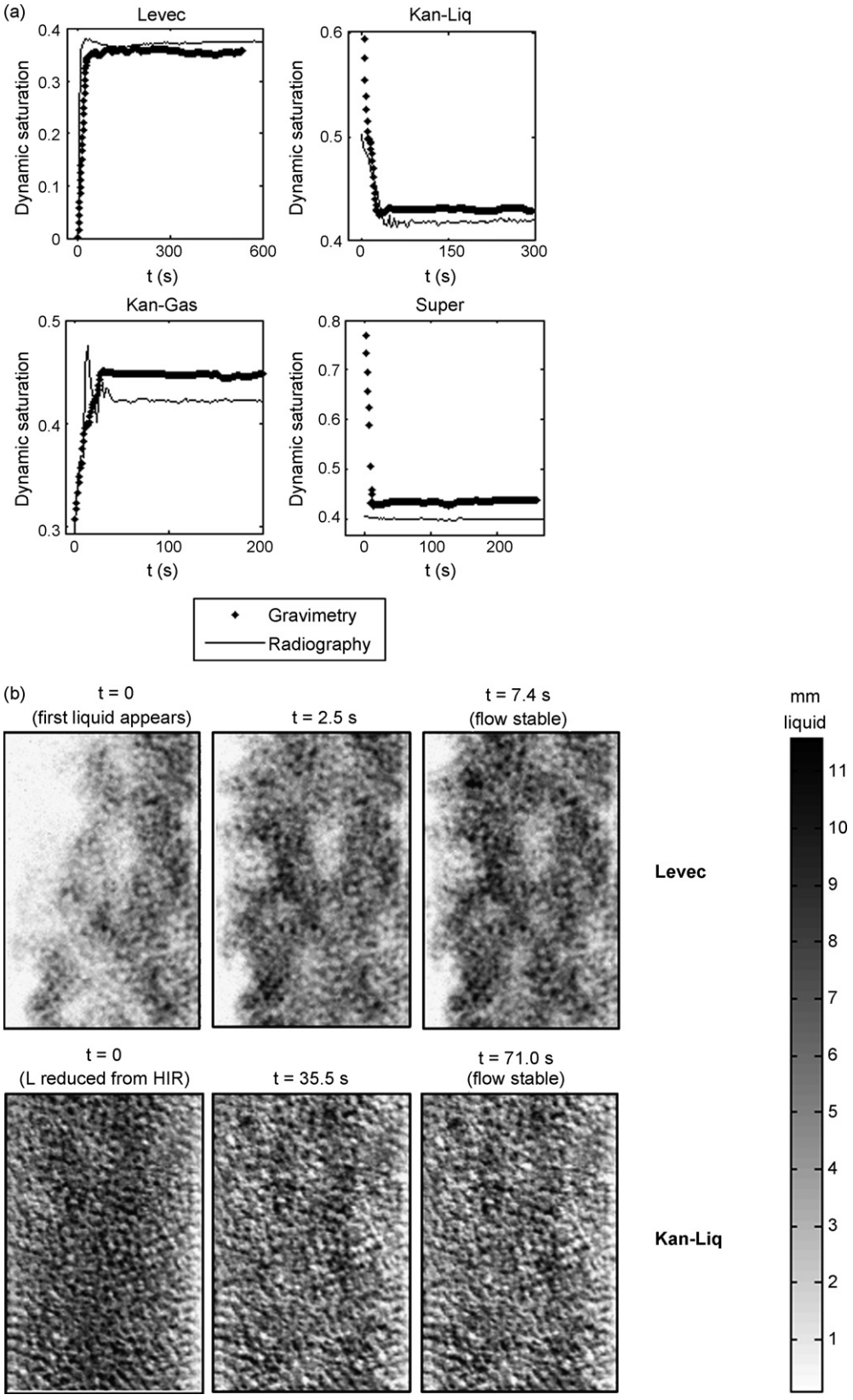

Fig. 6. Temporal saturation behaviour.

the start-up procedure, the nature of the packing and the inlet distribution. However, they only considered the non-pre-wetted and Super pre-wetted modes of operation [4]. Fig. 6(a) shows the temporal evolution of liquid saturation as registered by both the gravimetric and radiographic techniques employed in this study. Note that both techniques register the same dynamic behaviour of the liquid saturation shortly after start-up in each mode. Also evident from Fig. 6(a) is the fact that in these pre-wetting modes the saturation stabilized within 50–150 s. The non-pre-wetted mode failed to reach steady state even after 4 h of operation. Therefore, non-pre-wetted mode results are not reported elsewhere in this paper.

The differences in saturation for the different modes are in agreement with numerous studies on hydrodynamic hysteresis [21–27].

The rapidity of the saturation stabilization in the Levec, Kan and Super modes is further illustrated in Fig. 6(b). It shows successive radiographs of Levec and Kan-Liq pre-wetted beds. Based on these, it appears that the Levec bed reaches a stable configuration within 10 s after the first liquid appears in the field of view. The Kan-Liq bed reaches its stable configuration approximately 70 s after the liquid flow rate was reduced from its high value. The Super and Kan-Gas modes had similar dynamics to that of the Kan-Liq mode and are not shown for the sake of brevity.

4.3. Temporal stability at "steady state"

The stability of the liquid configurations in the various pre-wetting modes over longer times can now be tested using the radiographic technique. Although the term steady state implies no change with time in any variable, it is interesting to investigate whether it is possible to have liquid path variations without necessarily changing the global parameter values. For each of the operating points, 200 consecutive radiographs approximately 2 s apart (spanning a total of 8 min of operation) were monitored for flow path changes. The 8 min were taken from a period where the bed-averaged liquid saturation showed no substantial change. In order to more clearly show local saturation changes, the first image is subtracted from the

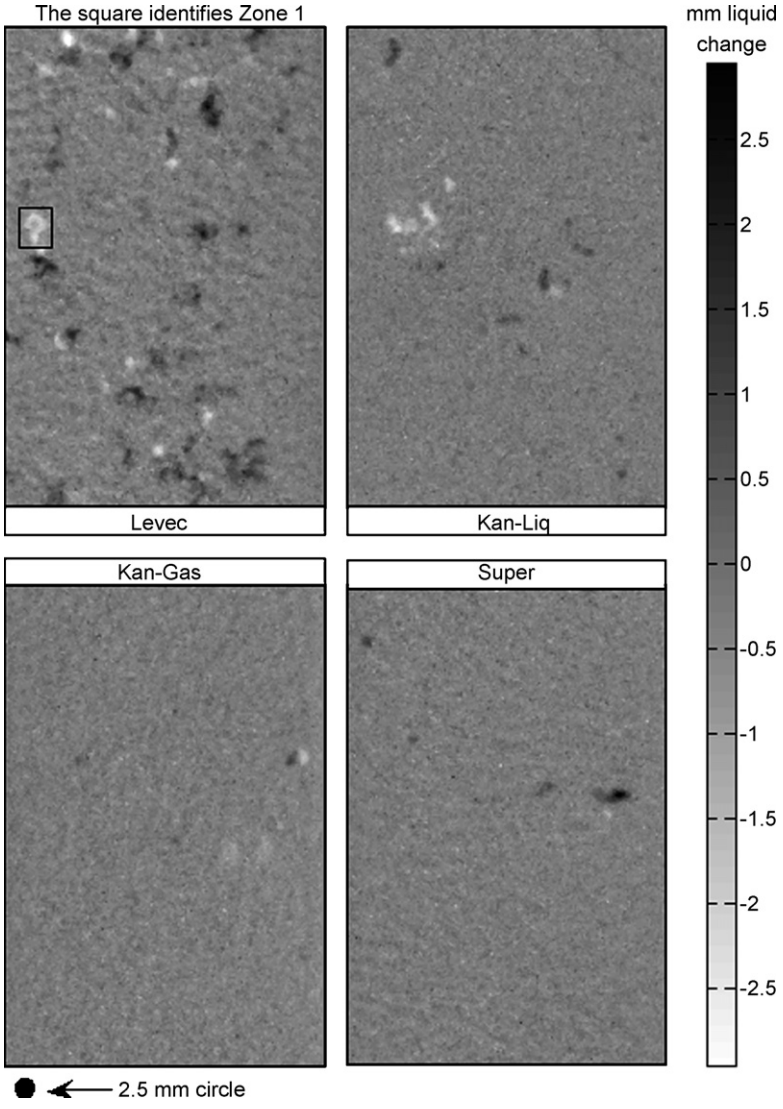

Fig. 7. Difference maps ($L = 8.0\,kg/m^2\,s$ and $G = 0.016\,kg/m^2\,s$).

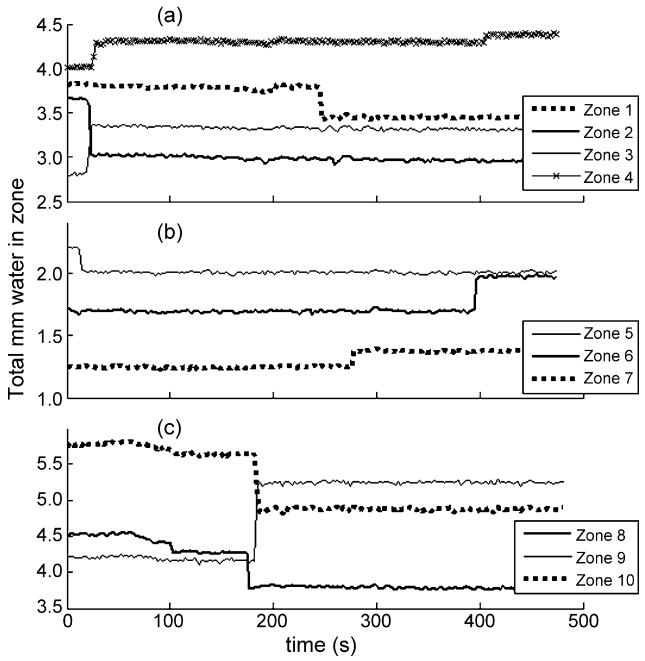

Fig. 8. Liquid saturation changes in different zones showing the size and frequency of changes: (a) $L = 5.3\,kg/m^2\,s$ and $G = 0.016\,kg/m^2\,s$; (b) $L = 1.3\,kg/m^2\,s$ and $G = 0.047\,kg/m^2\,s$; (c) $L = 5.3\,kg/m^2\,s$ and $G = 0.047\,kg/m^2\,s$.

last—yielding a difference map (i.e. difference map = steady-state image #200 − steady-state image #1). These are shown in Fig. 7. The dark areas in these images indicate locations where the saturation had a net increase during the 8 min, while the light (white) areas indicate a net decrease. Several millimetres (maximum of 3.4 mm) of change register at multiple locations in the Levec pre-wetted bed. Considering that there is a maximum of approximately 12 mm water at any given location (Fig. 3) at these flow rates, this represents a large change in local saturation. Interestingly, there are almost no such saturation changes in the other pre-wetting modes. Very similar difference maps are obtained at other liquid and gas flow rates (not shown).

Additional characteristics of the saturation perturbations in the Levec mode are revealed by the difference maps. The length scale appears to be very close to one particle diameter (a single particle diameter is shown at the bottom of Fig. 7 in direct proportion to the radiograph). There are both increases and decreases in local saturation and these seem to cancel each other out so that the bed-average value remains nearly constant. In the Kan-Liq, Kan-Gas and Super modes the flow pattern remains stable. The locations of temporal instability in the Levec mode are subsequently referred to as unstable zones. Having established the locations of these unstable zones, they can be monitored by examining consecutive radiographs (2 s apart) to establish when the liquid saturation change(s) occurred, how long such a change takes and whether it is a single change or multiple oscillations at that location. One way of illustrating this is to plot the total liquid thickness in an unstable zone against time. Fig. 8(a) zone 1 is such a plot for the unstable zone marked in Fig. 7, clearly showing that there was one sudden de-saturation (at approximately 250 s). Fig. 8 also includes such plots for other unstable zones (also at other gas and liquid fluxes). Zones are numbered consecutively for convenience. Their exact locations are not important apart from the fact that they were all present only in the Levec pre-wetted mode. In these plots, step changes indicate sudden increases or decreases in local saturation. From all the timed data generated in this study, the following conclusions can be drawn:

- An increased saturation in one zone is sometimes (but not always) accompanied by a decreased saturation at another (close by). See for example Fig. 8(a) zones 2 and 3 and (c) zones 9 and 10. This suggests that the liquid had moved from one zone to the other.
- The change in saturation never takes longer than 5 s to complete (regardless of the flow velocities).
- The frequency of changes is very low (there are hundreds of seconds between changes).

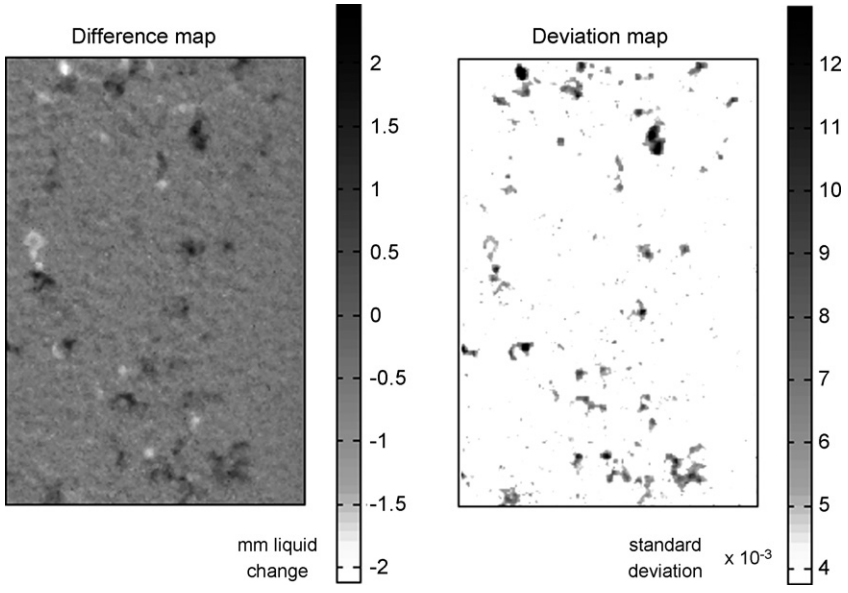

Fig. 9. Comparison between a difference map and a deviation map ($L = 8.0\,kg/m^2\,s$ and $G = 0.016\,kg/m^2\,s$).

- The same unstable zone sometimes experiences more than one saturation change (see zones 4 and 8 in Fig. 8(a) and (c), respectively). This suggests that there is some underlying aspect to the bed that can be associated with these saturation changes. However, at different flow rates it is not these same zones that undergo saturation changes (not shown).
- It cannot be concluded that either the frequencies of saturation changes or their magnitudes are linked to the liquid or gas flow rates.
- The local saturation changes in the Levec mode does not serve to increase the distribution uniformity and the flow pattern remains far removed from the Kan-Liq mode (at least for the longest time under investigation here: 2.5 h).

It is important to note that the difference maps employed here only shows the difference between the 200th and first images. As such, a difference map is incapable of registering saturation changes that cancel themselves out in the interval between the images used for its generation. That is, should a saturation increase somewhere in the bed be followed by a saturation decrease of the same magnitude within the 8 min it would not show on the difference map. However, such double (or multiple) changes do show on a standard deviation map which uses all of the images in the interval. These are calculated analogously to those of Anadon et al. [12]. Fig. 9 shows a comparison between a difference map and a deviation map for the Levec pre-wetted mode shown in Fig. 7. In every case presently under examination, the standard deviation maps and difference maps identified the same zones as unstable for the Levec mode. This means that there where no zones that had double changes of opposing sign and equal amplitude in the time period under investigation. In the other modes both the difference and the deviation maps indicate no dynamic changes in flow pattern. Consequently, difference maps are preferred because they are capable of showing whether an increase or a decrease in saturation had occurred while the standard deviation maps are not. It should be noted that the saturation changes reported here are not equivalent to those of Anadon et al. [12]. In their work, high frequency (several per second) localized saturation changes occurred in the Kan-Liq mode close to the trickle-to-pulse flow transition boundary. It was shown how these instabilities are to be considered the precursors of the pulsing regime [12]. In contrast, the low frequency instabilities reported in this study are inherent to the Levec mode in the trickle flow regime and occur at all velocities, but not in the Kan-Liq, Kan-Gas and Super modes.

4.4. Saturation and flow pattern reproducibility

For one set of gas and liquid flow rates, repeat runs for the Levec and Kan-Liq modes were conducted. These two modes are the most commonly employed in literature. Fig. 10(a) shows that in both pre-wetting modes the liquid saturation had completely reproducible temporal behaviour with little difference between the steady-state saturation values. However, close examination of the processed radiographs at steady state reveals that the liquid is not located at the same positions in the bed. This can be more clearly seen when the difference of two liquid saturation radiographs are taken (i.e. Run 1 radiograph–Run 2 radiograph) as shown in Fig. 10(b). Note that these runs were conducted directly after one another on exactly the same bed without moving it. Moreover, the same pre-wetting and operational procedures were followed. It is concluded that the liquid morphology is not exclusively determined by the bed structure and the pre-wetting method. However, both the total external saturation values and

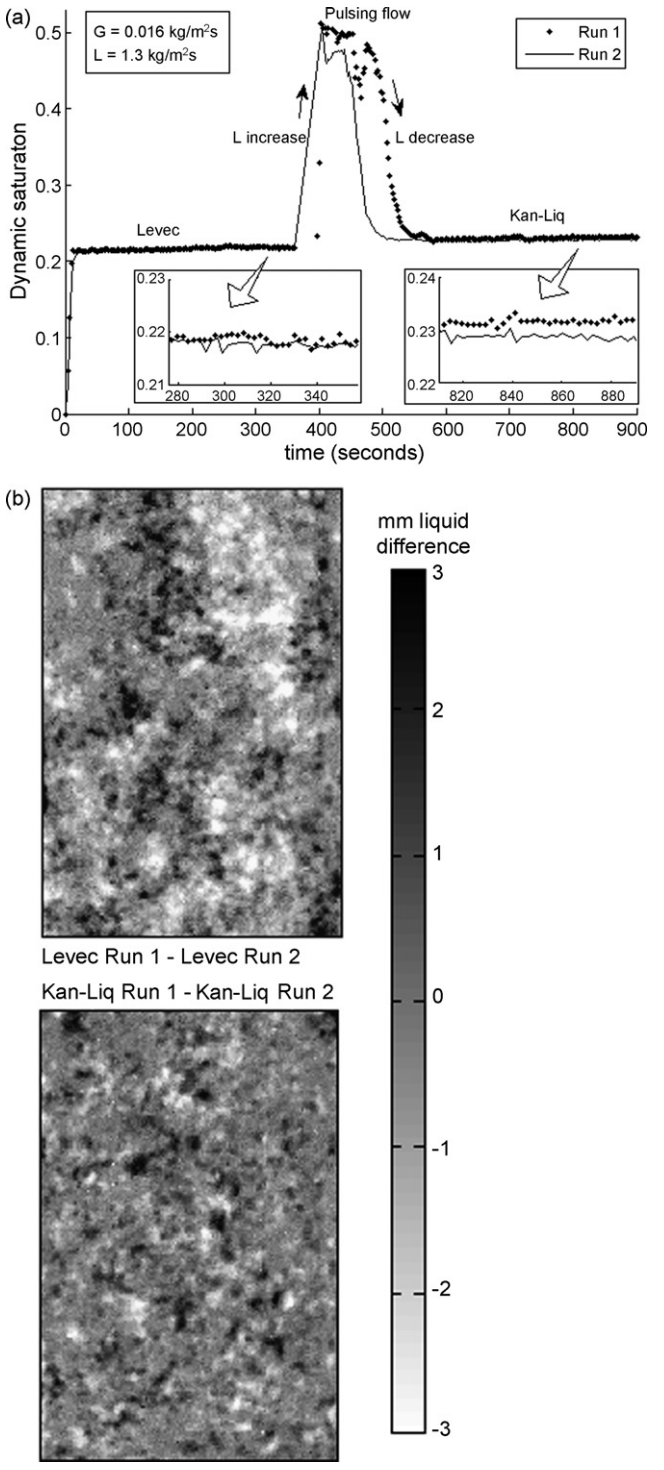

Fig. 10. Flow pattern and liquid saturation reproducibility: (a) saturation reproducibility; (b) liquid distribution reproducibility.

the general flow type are. This is true for both the Levec and Kan-Liq pre-wetted beds, although it is more apparent for the former. Lutran et al. [6] concluded that the flow pattern was reproducible given that the same pre-wetting procedure had been followed. However, examination of their Fig. 21 shows that although the general flow pattern was reproducible, the liquid was not located at exactly the same locations. It is therefore concluded that present results agree with those in Lutran et al. [6].

5. Conclusions

Radiographic imaging of trickle flow liquid saturation and distribution as a function of time, pre-wetting procedure and liquid and gas velocities is presented. A procedure to isolate the dynamic (free-draining) liquid from such images is introduced. The liquid saturation determined from these images is shown to agree with gravimetric liquid saturation measurements. This is encouraging since large diameter reactors are easier to radiograph than to weigh. The radiographic images indicate that the liquid saturation stabilizes shortly after the end of the start-up procedure for all pre-wetting modes except non-pre-wetted beds. Present results agree with previous investigators in that Levec beds have lower saturations and are dominated by non-uniform flow. These flow non-uniformities persist at high liquid and gas flow rates. Although the bed-averaged liquid saturation and general flow type (sometimes referred to as rivulets for Levec pre-wetted beds and films for Kan and Super beds) are completely reproducible, the exact location of the liquid in the bed appears to have a stochastic nature. It has been established that there are local saturation changes (without changing the bed-averaged values) in the Levec mode, but not in the Kan-Liq, Kan-Gas or Super modes. These changes are sudden but with a low frequency, occur at both high and low liquid and gas flow rates and do not appear to alter the general flow type. Apart from these small perturbations in this one mode the overall flow structure remains stable for several hours, suggesting that the different modes of operation will prevail for longer operating times. These observations form the basis of an ongoing computed tomography study of trickle flow in the various pre-wetting modes. In summary, the capabilities of X-ray radiography (in particular its high temporal resolution) have been used to provide new insights into the stability and uniformity of trickle flow in several hydrodynamic states.

Acknowledgements

The authors thank Sasol Technology Research and Development and the National Research Foundation of South Africa for ongoing financial support, as well as the South African Nuclear Energy Corporation for the use of its facilities.

References

[1] C.N. Satterfield, Trickle-bed reactors, AIChE J. 21 (2) (1975) 209–228.
[2] C.L. Lazzaroni, H.R. Keselman, N.S. Figoli, Colorimetric evaluation of the efficiency of liquid–solid contacting in trickle flow, Ind. Eng. Chem. Res. 27 (1988) 1132–1135.
[3] C.L. Lazzaroni, H.R. Keselman, N.S. Figoli, Trickle bed reactors. Multiplicity of hydrodynamic states. Relation between the pressure drop and the liquid holdup, Ind. Eng. Chem. Res. 28 (1989) 119–121.
[4] P.V. Ravindra, D.P. Rao, M.S. Rao, Liquid flow texture in trickle-bed reactors: an experimental study, Ind. Eng. Chem. Res. 36 (1997) 5133–5145.
[5] A.J. Van Houwelingen, C. Sandrock, W. Nicol, Particle wetting distributions in trickle bed reactors, AIChE J. 52 (2006) 3532–3542.
[6] P.G. Lutran, K.M. Ng, E.P. Delikat, Liquid distribution in trickle beds. An experimental study using computer-assisted tomography, Ind. Eng. Chem. Res. 30 (1991) 1270–1280.
[7] D. Toye, P. Marchot, M. Crine, A.-M. Pelsser, G. L'Homme, Local measurements of void fraction and liquid holdup in packed columns using X-ray computed tomography, Chem. Eng. Proc. 37 (1998) 511–520.
[8] M.D. Mantle, A.J. Sederman, L.F. Gladden, Single- and two-phase flow in fixed-bed reactors: MRI flow visualisation and Lattice–Boltzmann simulations, Chem. Eng. Sci. 56 (2001) 523–529.
[9] A.J. Sederman, L.F. Gladden, Magnetic resonance imaging as a quantitative probe of gas–liquid distribution and wetting efficiency in trickle-bed reactors, Chem. Eng. Sci. 56 (2001) 2615–2628.
[10] C. Boyer, B. Fanget, Measurement of liquid flow distribution in trickle bed reactor of large diameter with a new gamma-ray tomographic system, Chem. Eng. Sci. 57 (2002) 1079–1089.
[11] P. Marchot, D. Toye, A.-M. Pelsser, M. Crine, G. L'Homme, Z. Olujic, Liquid distribution images on structured packing by X-ray computed tomography, AIChE J. 47 (2001) 1471–1476.
[12] L.D. Anadon, M.H.M. Lim, A.J. Sederman, L.F. Gladden, Hydrodynamics in two-phase flow within porous media, Magn. Reson. Imag. 23 (2005) 291–294.
[13] L.F. Gladden, P. Alexander, M.M. Britton, M.D. Mantle, A.J. Sederman, E.H.L. Yuen, In situ magnetic resonance measurement of conversion, hydrodynamics and mass transfer during single- and two-phase flow in fixed-bed reactors, Magn. Reson. Imag. 21 (2003) 213–219.
[14] A. Kantzas, Computation of holdups in fluidized and trickle beds by computer-assisted tomography, AIChE J. 40 (1994) 1254–1261.
[15] N. Reinecke, D. Mewes, Tomographic imaging of trickle-bed reactors, Chem. Eng. Sci. 51 (1996) 2131–2138.
[16] C.E. Schmit, D. Cartmel, R.B. Eldridge, Process tomography: an option for the enhancement of packed vapor–liquid contactor model development, Ind. Eng. Chem. Res. 39 (2000) 1546–1553.
[17] F. Yin, A. Afacan, K. Nandakumar, K.T. Chuang, Liquid holdup distribution in packed columns: gamma ray tomography and CFD simulation, Chem. Eng. Proc. 41 (2002) 473–483.
[18] L.F. Gladden, M.H.M. Lim, M.D. Mantle, A.J. Sederman, E.H. Stitt, MRI visualisation of two-phase flow in structured supports and trickle-bed reactors, Catal. Today 79/80 (2003) 203–210.
[19] M.G. Basavaraj, G.S. Gupta, K. Naveen, V. Rudolph, R. Bali, Local liquid holdups and hysteresis in a 2D packed bed using X-ray radiography, AIChE J. 51 (2005) 2178–2189.
[20] M.G. Basavaraj, G.S. Gupta, New calibration technique for X-ray absorption studies in single and multiphase flows in packed bed, ISI J. Int. 44 (2004) 50–58.
[21] C. Marcandelli, A.S. Lamine, J.R. Bernard, G. Wild, Liquid distribution in trickle-bed reactor, Oil Gas Sci. Technol. 55 (2000) 407–415.
[22] K.M. Kan, P.F. Greenfield, Multiple hydrodynamic states in cocurrent two-phase down-flow through packed beds, Ind. Eng. Chem. Process Des. Dev. 17 (1978) 482–485.
[23] K.M. Kan, P.F. Greenfield, Pressure drop and holdup in two-phase cocurrent trickle flows through packed beds, Ind. Eng. Chem. Process Des. Dev. 18 (1979) 740–745.
[24] G. Christensen, S.J. McGovern, S. Sundaresan, Cocurrent downflow of air and water in a two-dimensional packed column, AIChE J. 32 (10) (1986) 1677–1689.
[25] J. Levec, K. Grosser, R.G. Carbonell, The hysteretic behaviour of pressure drop and liquid holdup in trickle beds, AIChE J. 34 (1988) 1027–1030.
[26] R. Wang, Z. Mao, J. Chen, Experimental and theoretical studies of pressure drop hysteresis in trickle bed reactors, Chem. Eng. Sci. 50 (14) (1995) 2321–2328.

[27] D.S. Loudon, W. Van der Merwe, W. Nicol, Multiple hydrodynamic states in trickle flow: the effect of prewetting procedure on liquid holdup. Pressure drop and gas–liquid mass transfer, Chem. Eng. Sci. 61 (2006) 7551–7562.
[28] P.J. Hoek, J.A. Wesselingh, F.J. Zuiderweg, Small scale and large scale liquid maldistribution in packed columns, Chem. Eng. Res. Des. 64 (1986) 411.
[29] D. Toye, P. Marchot, M. Crine, G. L'Homme, Analysis of liquid flow distribution in trickling flow reactor using computer assisted X-ray tomography, Chem. Eng. Res. Des. 77 (1995) 511–518.
[30] F.C. De Beer, Characteristics of the neutron/X-ray tomography system at the SANRAD facility in South Africa, Nucl. Instrum. Methods Phys. Res. A 542 (2005) 1–8.
[31] A. Burghardt, G. Bartelmus, M. Jaroszynski, A. Kolodziej, Hydrodynamics and mass transfer in a three-phase fixed-bed reactor with cocurrent gas–liquid downflow, Chem. Eng. J. 58 (1995) 83–99.
[32] W. Van der Merwe, W. Nicol, F.C. De Beer, Internal wetting dynamics of alpha- and gamma-alumina catalyst spheres using X-Ray computed tomography. S.A. J. Sci., in press.
[33] A. Gianetto, V. Specchia, Trikcle-bed reactors: state of art and perspectives, Chem. Eng. Sci. 47 (1992) 3197–3213.
[34] http://physics.nist.gov/PhysRefData/XrayMassCoef/ComTab/water.html (July 11, 2006).
[35] D. Nemec, G. Bercic, J. Levec, Gravimetric method for the determination of liquid holdup in pressurized trickle-bed reactors, Ind. Eng. Chem. Res. 40 (2001) 3418–3422.
[36] W. Van der Merwe, W. Nicol, Characterization of multiple flow morphologies within the trickle flow regime, Ind. Eng. Chem. Res. 44 (2005) 9446–9450.
[37] M.H. Al-Dahhan, M.P. Dudukovic, Catalyst wetting efficiency in trickle-bed reactors at high pressure, Chem. Eng. Sci. 50 (1995) 2377–2389.